J. Fluid Mech. (2025), *vol.* 1011, R1, doi:10.1017/jfm.2025.361



Knowledge-integrated additive learning for consistent near-wall modelling of turbulent flows

Fengshun Zhang[1,2], **Zhideng Zhou**[1,2], **Xiaolei Yang**[1,2] and **Guowei He**[1,2]

[1]The State Key Laboratory of Nonlinear Mechanics, Institute of Mechanics, Chinese Academy of Sciences, Beijing 100190, PR China

[2]School of Engineering Sciences, University of Chinese Academy of Sciences, Beijing 100049, PR China

Corresponding author: Xiaolei Yang, xyang@imech.ac.cn

(Received 24 January 2025; revised 1 March 2025; accepted 23 March 2025)

Developing a consistent near-wall turbulence model remains an unsolved problem. The machine learning method has the potential to become the workhorse for turbulence modelling. However, the learned model suffers from limited generalisability, especially for flows without similarity laws (e.g. separated flows). In this work, we propose a knowledge-integrated additive (KIA) learning approach for learning wall models in large-eddy simulations. The proposed approach integrates the knowledge in the simplified thin-boundary-layer equation with a data-driven forcing term for the non-equilibrium effects induced by pressure gradients and flow separations. The capability learned from each flow dataset is encapsulated using basis functions with the corresponding weights approximated using neural networks. The fusion of capabilities learned from various datasets is enabled using a distance function, in a way that the learned capability is preserved and the generalisability to other cases is allowed. The additive learning capability is demonstrated via training the model sequentially using the data of the flow with pressure gradient but no separation, and the separated flow data. The capability of the learned model to preserve previously learned capabilities is tested using turbulent channel flow cases. The periodic hill and the 2-D Gaussian bump cases showcase the generalisability of the model to flows with different surface curvatures and different Reynolds numbers. Good agreements with the references are obtained for all the test cases.

Key words: machine learning, turbulence modelling

1. Introduction

Large-eddy simulation (LES) has the potential to become an essential tool in the computational fluid dynamics (CFD) software for industrial applications (Slotnick *et al.* 2014). Wall models are crucial for LES to achieve its goal (Choi & Moin 2012; He, Jin &

© The Author(s), 2025. Published by Cambridge University Press.

https://doi.org/10.1017/jfm.2025.361 Published online by Cambridge University Press

Yang 2017; Yang & Griffin 2021). However, the classic wall models, relying on the law of walls, are only applicable to attached flows (Piomelli & Balaras 2002; Bose & Park 2018). Therefore, developing a consistent wall model suitable for both attached and separated flows has become a long-standing aspiration in the LES community. The machine learning method, and in particular the deep neural network, has emerged as a powerful tool for near-wall modelling due to its strong expression capabilities (Milano & Koumoutsakos 2002; Yang *et al.* 2019; Zhou, He & Yang 2021). Nevertheless, wall models trained using certain flow data face challenges in consistently performing well for other flow states. For example, a model trained using attached flow may not generalise well to separated flows. In this work, we are dedicated to developing a near-wall modelling approach for consistent predictions of both attached and separated flows.

A wall model represents the impacts of the unresolved near-wall flow on the outer flow using approximate boundary conditions, e.g. the wall shear stress τ_w, thereby avoiding the need to resolve the small-scale near-wall eddies. In classic wall models, the law of the wall (Piomelli & Balaras 2002; Zhang *et al.* 2022) is employed for estimating the wall shear stress. However, for separated flows, a general form of the law of the wall has yet to be established. Particularly, the characteristic velocity in the law of the wall, defined as $u_\tau = \sqrt{\tau_w/\rho}$ (where ρ denotes the fluid density), becomes ill-defined for separated flows. To solve the problem, the pressure gradient is employed to define an alternative characteristic velocity (Duprat *et al.* 2011). However, merely modifying the characteristic velocity cannot account for the mechanisms driving flow separation. A more comprehensive approach involves solving the simplified forms of the Navier–Stokes equations, such as the thin-boundary-layer (TBL) equations. The TBL equation can be further simplified to the so-called simplified thin-boundary-layer (TBL-s) equation (Cabot & Moin 2000; Wang & Moin 2002), which retains only the viscous term in the wall-normal direction. The primary advantage of the TBL-s equation lies in its reduction to an ordinary differential equation (ODE), which can be efficiently solved locally in the wall-normal direction. However, both the TBL and TBL-s equations are inadequate for modelling separated flows, as the terms neglected are of the same order as the retained terms when strong interactions occur between the near-wall and outer region in separated flows.

The machine learning method can effectively build the correlation between the near-wall flow and the wall shear stress. However, it faces significant challenges, particularly, (i) lack of generalisability: it is the problem that a model trained using a finite set of flow data is not guaranteed to work for a wide range of flows and to respect the law of the wall, in which the latter has been highlighted in two recent papers (Vadrot *et al.* 2023*a*,*b*); (ii) limited computational power: it occurs, if a model applicable to a wide range of attached and separated flows is trained once, that the amount of flow data becomes prohibitively huge. To address the challenges, several works have been carried out in the literature. In the building-block-flow wall model (Lozano-Durán & Bae 2023; Arranz *et al.* 2024), the data of several canonical flows are employed to train the model, showing overall good agreements with references for several attached turbulent flows and two realistic aircraft configurations. The key assumption of their approach is that a complex flow state can be represented using several canonical flows. In the feature-embedded learning approach proposed in our prior work (Zhou *et al.* 2021, 2023*b*, 2025), the philosophy, on the other hand, is that a model learned from the two extremes, e.g. the attached flow and the separated flow, is applicable to flow states in between. Specifically, the data from periodic hill simulations and the law of the wall were employed to train a neural network model for predicting wall shear stress, showing successful applications to turbulent channel flows at various Reynolds numbers and several kinds of unseen separated flows.

https://doi.org/10.1017/jfm.2025.361 Published online by Cambridge University Press

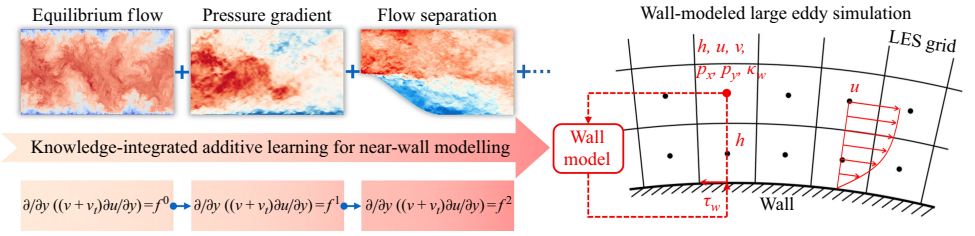


Figure 1. Schematic of the proposed KIA approach.

In this work, we propose a novel continual learning approach featured by 'easy to generalise' and 'low computational demands'. It integrates the knowledge of an ODE (i.e. the TBL-s equation) with data-driven models via a nonlinear forcing term, additively improving the model's capabilities. The proposed learning approach has two important features: the encapsulation and fusion capabilities. The core assumption of the proposed approach is that, with a limited number of basis functions, the ODE with a nonlinear forcing term can capture the essential physics of both attached and separated flows. It reduces the computational demand by allowing case-after-case learning and avoids the issue of 'catastrophic forgetting' with the use of distance functions to preserve the previously learned capabilities while learning new ones. To test the approach, the model is trained additively using high-fidelity simulation data, starting with the flow data featured by pressure gradients without separation, followed by the separated flow data. The obtained results demonstrate that the model can effectively learn new capabilities in a case-after-case manner, with the previously learned capabilities well preserved. Furthermore, the model exhibits strong *a posteriori* performance across diverse flow configurations, highlighting its potential for robust and consistent near-wall modelling. It is noted that the approach proposed in this work and the progressive machine learning method employed by Bin *et al.* (2022) share the same goal of learning a near-wall model from simple to complex flows without catastrophic forgetting. The key difference between the two lies in the employed methodology, that the continual learning is enabled by augmenting a neural network in the work by Bin *et al.* (2022), while it is achieved in a modular form with separate neural networks for each flow dataset in the present work. Moreover, the work by Bin *et al.* (2022) was focused on learning the eddy viscosity model, while the present work aims at learning a consistent near-wall model for both attached and separated flows based on the TBL-s equation.

In the rest of the paper, the proposed approach is introduced in § 2, the results of the *a priori* and *a posteriori* tests are shown in §§ 3 and 4, respectively, and the conclusions are drawn in § 5.

2. Knowledge-integrated additive learning of the wall model

The model assumes that the near-wall region of various flow states can be represented by an ODE for attached flows, augmented with a forcing term to account for non-equilibrium effects in flows with pressure gradients and separated flows. The proposed knowledge-integrated additive (KIA) learning approach learns the forcing term in a case-after-case manner (figure 1). It begins with a baseline ODE for attached flows, for which the viscous term dominates, and additively learns the forcing term to account for the neglected effects. The case-after-case continual learning without catastrophic forgetting is enabled by the encapsulation and fusion capabilities of the proposed approach:

https://doi.org/10.1017/jfm.2025.361 Published online by Cambridge University Press

(i) The encapsulation capability allows a modular-form model learned for each case, which consists of the predefined basis functions and neural networks for their coefficients. The basis functions define how the non-equilibrium effects are represented, while the neural networks model how different basis functions act when simulating a certain flow state.

(ii) The fusion capability synthesises models learned from various flow datasets by introducing a distance function. This distance function measures how effectively the existing model represents the new flow dataset, ensuring that only the previously unrepresented data are learned and the model's previously acquired capabilities are preserved.

The employed TBL-s equation with a forcing term $f(\boldsymbol{u}, p)$ where $\mathbf{u}$ is velocity vector, p is the pressure is in the following form,

$$\mathcal{F}(\boldsymbol{u}, p) = \frac{\partial}{\partial y}\left[(\nu + \nu_t)\frac{\partial u}{\partial y}\right] - f(\boldsymbol{u}, p) = 0, \tag{2.1}$$

where $\mathbf{u}$ is velocity vector, p is pressure, ν is kinematic viscosity, and u is the velocity parallel to the wall. The eddy viscosity ν_t in (2.1) is modelled using Prandtl's linear mixing length model with van Driest damping function (Pope 2000),

$$\nu_t = \nu\kappa y^* \left(1 - \mathrm{e}^{-y^*/A}\right)^2, \tag{2.2}$$

where Kármán constant $\kappa = 0.4$, $A = 17$, $y^* = yu_{\tau p}/\nu$, y denotes the wall-normal coordinate, and $u_{\tau p} = \sqrt{u_\tau^2 + u_p^2}$ with $u_p = |(\nu/\rho)(\partial p/\partial x)_h|^{1/3}$ the characteristic velocity defined using the pressure gradient in the tangential direction (Manhart, Peller & Brun 2008), with h for the sampling height of the wall model (which is defined at the center of the first cell off the wall in this work).

The forcing term f is approximated using the data-driven counterpart f^J (where J denotes the number of flow datasets additively employed for training), with the corresponding ODE denoted by $\mathcal{F}^J$. In this work, the f^J is in the following form:

$$f^J = \underbrace{\sum_{n=0}^{N}\phi_n(y)C_n^1(\mathcal{D}^1, \mathcal{F}^0)}_{\text{learned from flow dataset 1}} + \underbrace{\sum_{n=0}^{N}\phi_n(y)C_n^2(\mathcal{D}^2, \mathcal{F}^1)}_{\text{learned from flow dataset 2}} + \underbrace{\sum_{n=0}^{N}\phi_n(y)C_n^3(\mathcal{D}^3, \mathcal{F}^2)}_{\text{learned from flow dataset 3}} + \ldots \tag{2.3}$$

$$= \underbrace{\phi_0(y)\sum_{j=0}^{J}C_0^j(\mathcal{D}^j, \mathcal{F}^{j-1})}_{\text{basis function 1}} + \underbrace{\phi_1(y)\sum_{j=0}^{J}C_1^j(\mathcal{D}^j, \mathcal{F}^{j-1})}_{\text{basis function 2}} + \underbrace{\phi_2(y)\sum_{j=0}^{J}C_2^j(\mathcal{D}^j, \mathcal{F}^{j-1})}_{\text{basis function 3}} + \ldots, \tag{2.4}$$

where ϕ_n is the predefined basis function, $\mathcal{D}^j$ represents the jth flow dataset, C_n^j is the coefficient for the basis function ϕ_n at jth learning. In equations (2.3) and (2.4), the forcing term is written in two different forms, (i) case-wisely in the first equation, and (ii) basis-function-wisely in the second equation. The case-wise form indicates that the forcing term is expanded according to flow datasets. The basis-function-wise form signifies that the forcing term consists of a set of basis functions, with coefficients learned from various flow datasets. Different forms of basis functions can be employed. In this work, the basis function is of a polynomial form as follows:

$$\phi_n = \left(\frac{y}{h}\right)^n, \tag{2.5}$$

https://doi.org/10.1017/jfm.2025.361 Published online by Cambridge University Press

where h represents the wall-normal distance for the first off-wall grid node. Although each basis function cannot be related to a specific flow regime because of the complexity of the flow, we argue that the polynomial-form basis functions provide a universal way for approximating the non-equilibrium effects. The coefficient C_n^j for the basis function is computed via

$$C_n^j = c_n^j D_n^j, \tag{2.6}$$

where the coefficient c_n^j models the added flow data, and the distance function D_n^j measures how well the new data are represented using the existing model. The distance function D_n^j in (2.6) equals zero if the new flow data can already be described by the model previously learned. In this work, the distance function D_n^j is in the following form:

$$D_n^j = 1 - \mathrm{e}^{-\left(B_n^j\right)^2 \left| \frac{\tau_{w,r}^j - \tau_w^{j-1}\left(\mathcal{D}^{j-1}, \mathcal{F}^{j-1}\right)}{A_h U_b} \right|^2}, \tag{2.7}$$

where $\tau_{w,r}^j$ is the real wall shear stress from flow data set $\mathcal{D}^j$, B_n^j is the coefficient to be learned, $A_h = \rho / \int_0^h \mathrm{d}y/\nu + \nu_t$, and U_b is the characteristic velocity for normalisation.

In these formulations, the undetermined coefficients c_n^j and B_n^j are modelled using a neural network with 5 hidden layers, each containing 20 neurons. In this work, the input features are $\ln(hU_b/\nu)$, wall curvature $\kappa_w h$, $\nu u_h/hU_b^2$, u_h^2/U_b^2, $u_h v_h/U_b^2$, the tangential pressure gradient $h/\rho U_b^2 \partial p/\partial x|_h$, and the normal pressure gradient $h/\rho U_b^2 \partial p/\partial y|_h$. Here, κ_w is the wall curvature, u_h is the velocity parallel to the wall, and v_h is the velocity normal to the wall. The activation function used in the hidden layers is the hyperbolic tangent function. In the input features, a single value of U_b, i.e. the bulk velocity, is employed at all spatial locations for the simulated canonical flows. For flows with complex configurations, a single value of U_b may become inappropriate, and a position-specific characteristic velocity is preferred. Dividing the flow into building blocks of canonical flows is one possible way (Lozano-Durán & Bae 2023). The other possible way is to use the local outer flow information, which, however, requires an unambiguous definition.

With the learned forcing term, (2.1) can be solved numerically to obtain the tangential velocity in the near-wall region using the velocity boundary conditions at the wall and at $y = h$ from the outer flow. In this work, the wall-shear-stress boundary condition is employed in the outer flow simulations. It is not necessary to have the velocity distribution in the near-wall region. Taking advantage of the polynomial-form basis functions, an explicit expression for the wall shear stress τ_w can be easily obtained by integrating (2.1) twice from the wall to h above the wall, and is given as follows:

$$\tau_w = A_h \left[U_h - \sum_{j=1}^{J} \left(h C_0^j \int_0^h \frac{\frac{y}{h}\mathrm{d}y}{\nu + \nu_t} + \frac{h}{2} C_1^j \int_0^h \frac{\left(\frac{y}{h}\right)^2 \mathrm{d}y}{\nu + \nu_t} + \dots \right) \right]. \tag{2.8}$$

3. *A priori* tests on the performance of KIA learning

The wall-resolved LES data of the periodic hill flow are employed for training and testing. The data employed for model training are from cases with Reynolds numbers $Re = 2800$, 5600, 10 595, 19 000 and the hill slope $\alpha = 1.0$. In total, approximately 78 000 data pairs from the upper wall region and the lower hill region are utilised for model learning, which span wall-normal distances from $y/H = 0.005$ to $y/H = 0.1$, where H

https://doi.org/10.1017/jfm.2025.361 Published online by Cambridge University Press

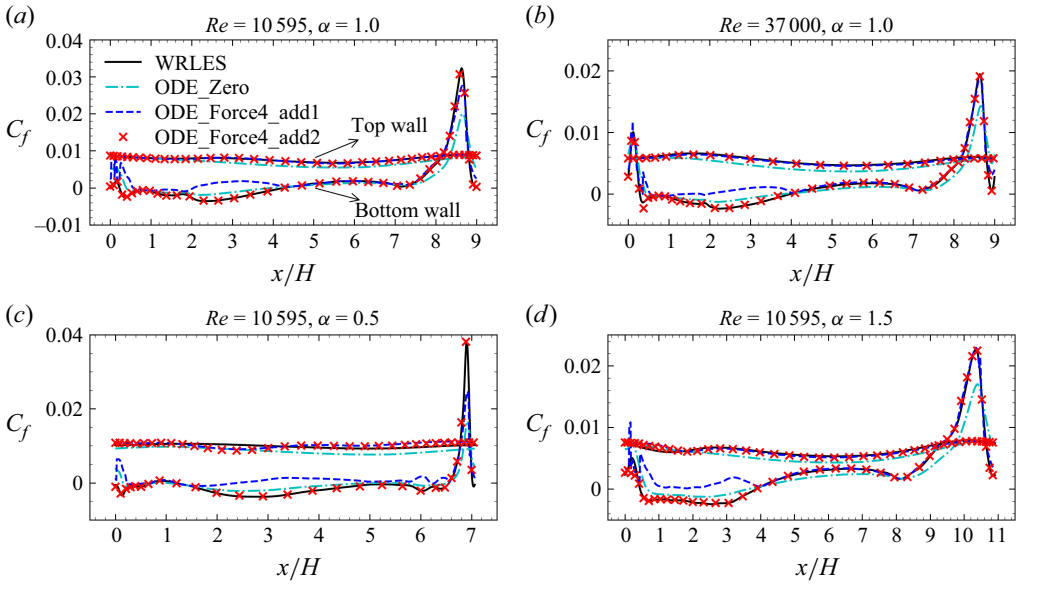


Figure 2. Performance of the models additively learned for one time (ODE_Force4_add1) and two times (ODE_Force4_add2) tested using the periodic hill cases. Time-averaged skin friction coefficients along the upper wall and lower hills for (*a*) $Re = 10\,595$ with $\alpha = 1.0$, (*b*) $Re = 37\,000$ with $\alpha = 1.0$, (*c*) $Re = 10\,595$ with $\alpha = 0.5$ and (*d*) $Re = 10\,595$ with $\alpha = 1.5$. WRLES denotes wall-resolved large-eddy simulation.

represents the height of hill, ensuring a comprehensive representation of the near-wall flow dynamics. The learning capability of the proposed approach is tested in *a priori* tests. The cases for model testing include (i) the periodic hill flow at a higher Reynolds number $Re = 37\,000$ with the hill slope $\alpha = 1.0$, and (ii) the two cases with different hill slopes $\alpha = 0.5$, 1.5 at Reynolds number $Re = 10\,595$. To test the additive learning capability, we separate the training data into two sets, i.e. the data near the upper wall and the data near the lower hills. Near the upper wall, the flow is featured by pressure gradients without flow separation, while it is characterised by a flow separation bubble near the lower hills. The baseline model is denoted as ODE_Zero. In the first additive learning, the flow data near the upper wall are employed, with the learned model dubbed as ODE_Force4_add1; in the second additive learning, the flow data near the lower hills are added to obtain the model ODE_Force4_add2. The number 4 in the model's name indicates that the employed basis functions are $\phi_0 = 1$, $\phi_1 = y/h$, $\phi_2 = (y/h)^2$, $\phi_3 = (y/h)^3$. More terms have been tested, showing no further improvements.

The model's performance is demonstrated in figure 2. It is seen that the baseline model, ODE_Zero, faces difficulty in predicting the wall shear stress on both the upper wall and the lower hills as expected. After the first additive learning using the upper wall data, the ODE_Force4_add1 model successfully predicts the time-averaged skin friction coefficients along the upper wall. At the lower hills, improvements were obtained in predicting the friction coefficient in the uphill region. Further improvements are achieved after the second additive learning using the data near the bottom hills. Overall, it has been shown that the model ODE_Force4_add2 additively learned twice has successfully retained its ability to predict wall shear stress at the upper wall and acquired the new capabilities to forecast C_f at the surface of the lower hills.

The final note in this section concerns the impact of the learning order on model accuracy. An additional test was conducted, where the model was first trained using the lower hill data and then the upper wall data. The results indicate no further improvements

https://doi.org/10.1017/jfm.2025.361 Published online by Cambridge University Press

Cases	Reynolds number	$L_x \times L_y \times L_z$	$N_x \times N_y \times N_z$	Δy_1
PH10 595-α1.0	$Re_H = 10\,595$	$9.0H \times 3.036H \times 4.5H$	$113 \times 33 \times 65$	$0.03H$
			$65 \times 33 \times 33$	$0.06H$
PH19 000-α1.0	$Re_H = 19\,000$	$9.0H \times 3.036H \times 4.5H$	$113 \times 33 \times 65$	$0.03H$
			$65 \times 33 \times 33$	$0.06H$
PH37 000-α1.0	$Re_H = 37\,000$	$9.0H \times 3.036H \times 4.5H$	$113 \times 33 \times 65$	$0.03H$
			$65 \times 33 \times 33$	$0.06H$
PH10 595-α0.5	$Re_H = 10\,595$	$7.07H \times 3.036H \times 4.5H$	$113 \times 33 \times 65$	$0.03H$
			$65 \times 33 \times 33$	$0.06H$
PH10 595-α1.5	$Re_H = 10\,595$	$10.93H \times 3.036H \times 4.5H$	$139 \times 33 \times 65$	$0.03H$
			$81 \times 33 \times 33$	$0.06H$

Table 1. Set-up of the periodic hill cases. Here, Re_H is based on the bulk velocity and the height of the hill (H), Δy_1 is the height of the first off-wall grid node. For each case, two grid resolutions are employed: the baseline and the coarse.

after the second learning phase, as the model trained on the lower hill data already performs well for both the upper wall and the lower hill in terms of the friction coefficient.

4. Applications to wall-modelled LES

One important feature of the learned model is that it can retain the capabilities previously learned. Specifically, the model additively learned using the periodic hill data should be able to revert to the ODE without a forcing term when it is applied to wall-bounded turbulent flows with the logarithmic law satisfied. This certainly happens in the *a priori* tests, but becomes complicated in the *a posteriori* tests, for which the inputs are from the instantaneous flow fields, and the discretisation errors and the subgrid-scale-model errors also play a role. Last, the model performance needs to be tested for flow configurations other than periodic hills.

In this section, we apply the learned model to wall-modelled LES of turbulent channel flows, flows over periodic hills, and the flow over a two-dimensional (2-D) Gaussian bump, with comparisons to the reference data from wall-resolved LES or experiments and the results from the traditional wall models. In the turbulent channel flow cases with the friction Reynolds number (which is defined using the friction velocity u_τ and the half-width of the channel δ) $Re_\tau = 1000, 2000, 5200$. The computational domain is $L_x \times L_y \times L_z = 7.0\delta \times 2.0\delta \times 3.5\delta$, where δ is the half-width of the channel, in the streamwise, vertical and spanwise directions, respectively. The number of grid nodes is $N_x \times N_y \times N_z = 33 \times 33 \times 33$. The height of the first off-wall grid cell is $\Delta y_1 = 0.0625\delta$. The parameters for the periodic hill cases are shown in table 1, for which systematic tests were carried out. In the Gaussian bump case, the simulation set-up follows our prior work (Zhou *et al.* 2025). The geometry is defined by the equation $y(x) = h\exp[-(x/x_0)^2]$, where the bump height $h = 0.085L$, the constant $x_0 = 0.195L$, and L represents the spanwise width of the three-dimensional bump configuration (Slotnick 2019). The Reynolds number, based on L and the upstream reference velocity U_∞, is $Re_L = 2 \times 10^6$. The computational domain is $L_x \times L_y \times L_z = 2.8L \times 0.5L \times 0.04L$ and is discretised using a grid with $N_x \times N_y \times N_z = 920 \times 91 \times 51$ nodes in the streamwise, vertical and spanwise directions, respectively. The first grid spacing in the vertical direction is $\Delta y_1 = 0.03h$.

The turbulent channel flow tests show good performance for all three Reynolds numbers $Re_\tau = 1000, 2000, 5200$. In figure 3, we show the turbulence statistics predicted by wall-modelled LES using the learned wall model for $Re_\tau = 5200$. As seen, the results from the

https://doi.org/10.1017/jfm.2025.361 Published online by Cambridge University Press

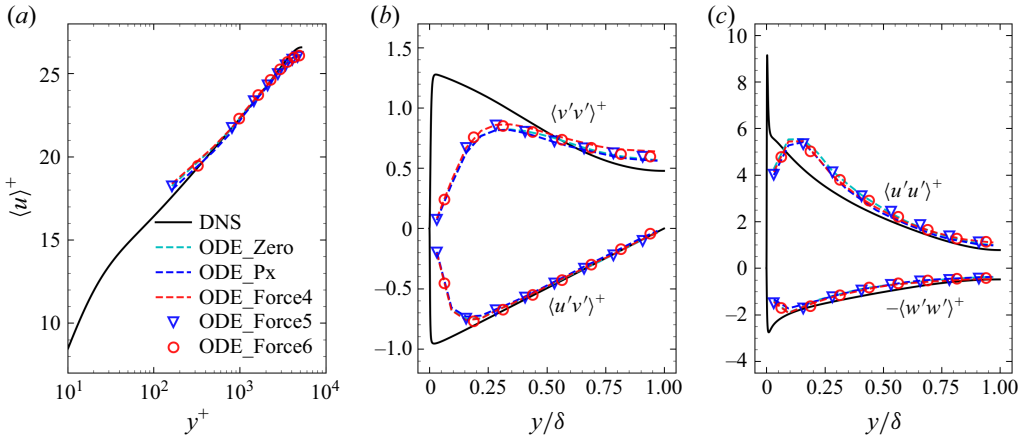


Figure 3. *A posteriori* tests using the turbulent channel flow case at Reynolds number $Re_\tau = 5200$ for (*a*) mean streamwise velocity, (*b*) primary Reynolds shear stress $\langle u'v' \rangle^+$ and wall-normal Reynolds normal stress $\langle v'v' \rangle^+$, (*c*) streamwise Reynolds normal stress $\langle u'u' \rangle^+$ and spanwise Reynolds normal stress $\langle w'w' \rangle^+$, where u', v', and w' represent the velocity fluctuations in the streamwise, wall-normal, and spanwise directions, respectively. The DNS data are from Lee & Moser (2015). The numerical value following the term 'Force' in the legend indicates the number of basis functions utilised.

learned model (i.e. ODE_Force4) show good agreement with the ODE_Zero model, the ODE_Px model (in which the forcing term f in Equation (2.1) only includes the tangential pressure gradient term), and the direct numerical simulation (DNS) data for the mean streamwise velocity. About the primary Reynolds shear stress, all the wall models closely align with the DNS data for $y/\delta > 0.2$, but underestimate the magnitude for $y/\delta < 0.2$. All the wall models exhibit good agreement with the DNS data for the Reynolds normal stresses in the outer region. Some discrepancies are observed in the near-wall region, especially for the vertical component ($\langle v'v' \rangle^+$). Overall, the learned model aligns well with the classical models (i.e. ODE_Zero, ODE_Px), demonstrating that it can retain the capabilities previously learned. Furthermore, similar performance is observed for the models learned with different numbers of basis functions.

The capability of the learned model for wall-modelled LES of separated flows is demonstrated via the periodic hill flow cases for Reynolds numbers higher than the training data and different hill slopes. The performance is first examined for the $Re = 37\,000$ case (case PH37 000-α1.0 in table 1), for which the Reynolds number is higher than the training flow data. Although some minor discrepancies exist in the separation bubble region for the turbulence kinetic energy as shown in figure 4, the learned models show an overall good agreement with the wall-resolved LES data for the time-averaged streamwise velocity ($\langle u \rangle$), vertical velocity ($\langle v \rangle$), primary Reynolds shear stress ($\langle u'v' \rangle$) and turbulence kinetic energy (k) for both grid resolutions. Figure 5 shows the time-averaged results of flow over periodic hills with hill slopes $\alpha = 0.5$ and $\alpha = 1.5$ (cases PH10 595-α0.5 and PH10 595-α1.5 in table 1), being different from the training flow data. As seen, in comparison with the baseline model, the ODE_Force4 model follows well the reference data for the time-averaged streamwise velocity and vertical velocity as well as the Reynolds shear stress and turbulence kinetic energy. The underprediction of the magnitude of k at certain streamwise locations is due primarily to the grid resolution employed in wall-modelled LES. The level of agreement improves when compared with the k values from filtered wall-resolved LES results, as demonstrated in our prior work (Zhou *et al.* 2025). The time-averaged skin friction coefficients from the wall-modelled LES are compared with the reference data

https://doi.org/10.1017/jfm.2025.361 Published online by Cambridge University Press

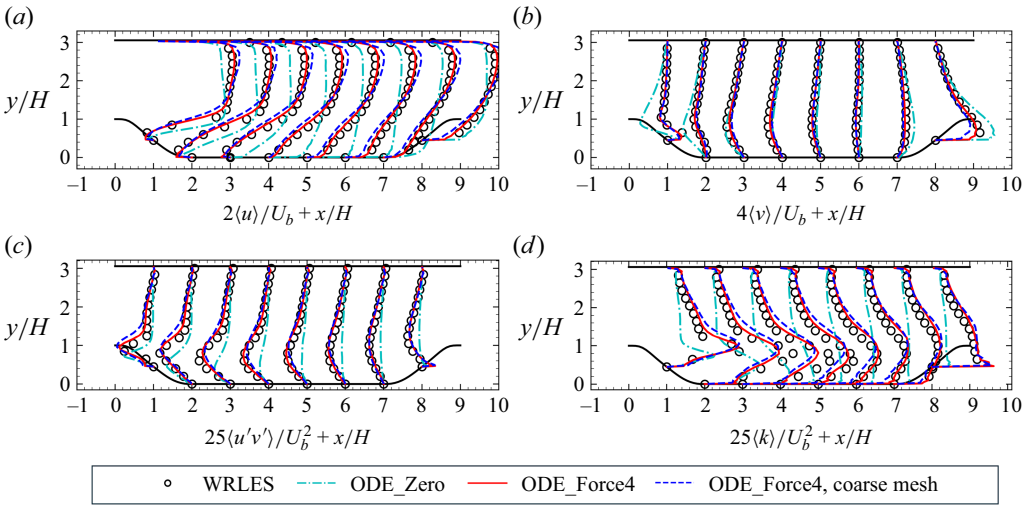


Figure 4. *A posteriori* tests using the periodic hill case at Reynolds number $Re = 37\,000$ higher than the training datasets for (*a*) time-averaged streamwise velocity, (*b*) time-averaged vertical velocity, (*c*) primary Reynolds shear stress, and (*d*) turbulence kinetic energy at Reynolds number $Re = 37\,000$. The reference wall-resolved LES data are from Zhou *et al.* (2023*a*).

in figure 6. While some discrepancies are observed at certain streamwise locations, the ODE_Force4 model achieves an overall good agreement.

To quantitatively assess the prediction accuracy of the proposed wall models, we compute the relative error at each streamwise location as follows:

$$err_q = \frac{\sum |q_{ref} - q_{wm}| \Delta y}{\sum |q_{ref}| \Delta y}, \tag{4.1}$$

where q denotes a flow quantity with the subscripts 'ref' and 'wm' for the reference and wall-modelled LES data, respectively. The prediction accuracy of the models is evaluated using the periodic hill cases, for which results are available across various models and grid resolutions. Specifically, the errors of the vertical profiles, shown in figures 4 and 5, are first computed at each streamwise location and then averaged for each case. The obtained errors are shown in figure 7. As observed, the errors are significantly reduced when comparing the results of the ODE_Force4 model with those of the ODE_Zero model for both grid resolutions. For the baseline grid, the average relative errors for the ODE_Force4 model are below 5 % for the mean streamwise velocity and under 20 % for the other three quantities, respectively.

The results from the 2-D Gaussian bump case are presented in figures 8 and 9. The four streamwise locations selected for comparison, i.e. $x/L = -0.4, -0.1, 0.1, 0.2$, correspond to regions with a mild adverse pressure gradient (APG), a strong favourable pressure gradient (FPG), a strong APG, and flow separation, respectively. As seen, the three models perform reasonably well at locations with APG and FPG. However, at the location downstream of the bump ($x/L = 0.2$), the ODE_Zero model fails to accurately predict the flow separation. For the ODE_Force4 model, although some discrepancies are observed around $y/L = 0.07$, it accurately predicts the vertical distribution of $\langle u \rangle$ in the flow separation region.

Interesting trends are observed in the comparison between the ODE_Force4 and FEL_{τ_w} predictions. Specifically, the ODE_Force4 model performs better in the upstream of the

https://doi.org/10.1017/jfm.2025.361 Published online by Cambridge University Press

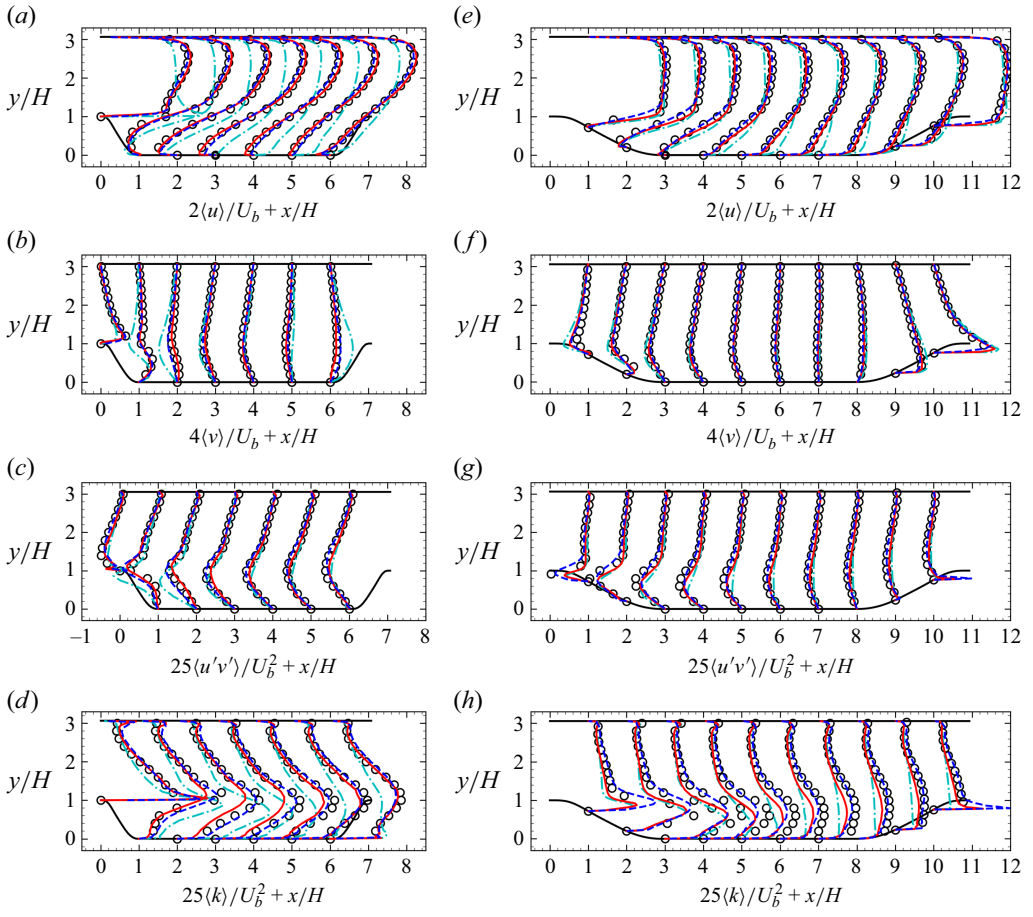


Figure 5. *A posteriori* tests using the periodic hill cases with hill slopes different from the training datasets and Reynolds number $Re = 10\,595$ for (*a*,*e*) time-averaged streamwise velocity, (*b*,*f*) time-averaged vertical velocity, (*c*,*g*) primary Reynolds shear stress and (*d*,*h*) turbulence kinetic energy. The reference wall-resolved LES data are from Zhou *et al.* (2023*a*). The legend is the same as figure 4.

bump but is less accurate in the separation region, while the opposite is true for the FEL_{τ_w} model. This indicates that the history effect from the upstream flow (Bobke *et al.* 2017; Parthasarathy & Saxton-Fox 2023; Yang *et al.* 2024) plays a non-negligible role in the streamwise flow evolution. However, this effect is not explicitly included in either model and should be accounted for in future model development.

Lastly, the computational overhead is assessed for the ODE_Force4 model in comparison with the ODE_Zero model. The increase in the wall-clock time is found to be modest, with the ratio ranging from 1.02 for the channel case to 1.16 for the 2-D Gaussian bump case.

5. Conclusions

In this work, we proposed a KIA learning approach for consistently modelling the near-wall region of both attached and separated turbulent flows in LES, a long-standing challenge for LES. In the proposed approach, the learning of a wall model starts from an ODE, which describes the near-wall flow in the equilibrium state. The non-equilibrium

https://doi.org/10.1017/jfm.2025.361 Published online by Cambridge University Press

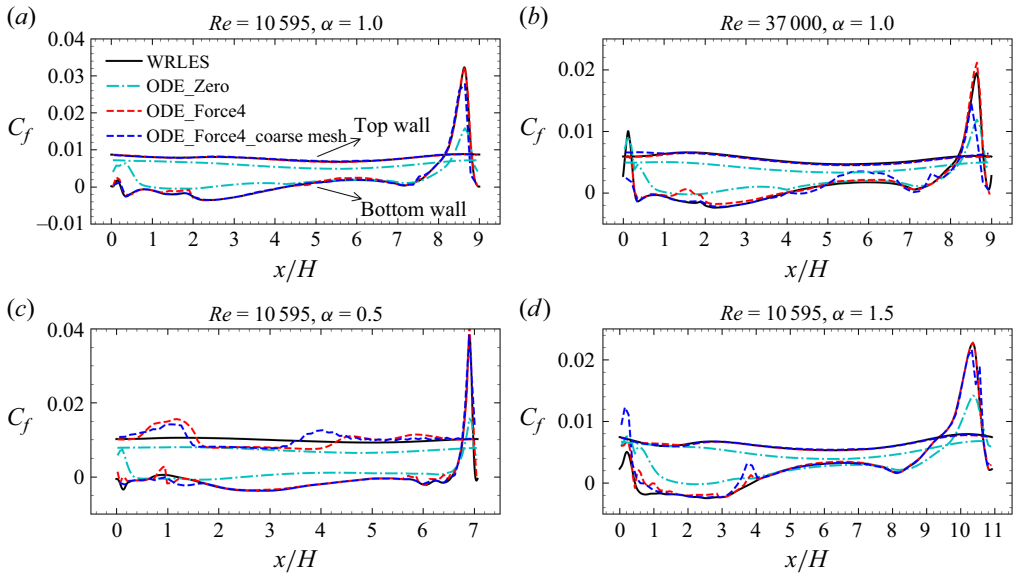


Figure 6. *A posteriori* tests using the periodic hill cases. Time-averaged skin friction coefficients along the upper wall and lower hills for (*a*) $Re = 10\,595$ with $\alpha = 1.0$, (*b*) $Re = 37\,000$ with $\alpha = 1.0$, (*c*) $Re = 10\,595$ with $\alpha = 0.5$ and (*d*) $Re = 10\,595$ with $\alpha = 1.5$.

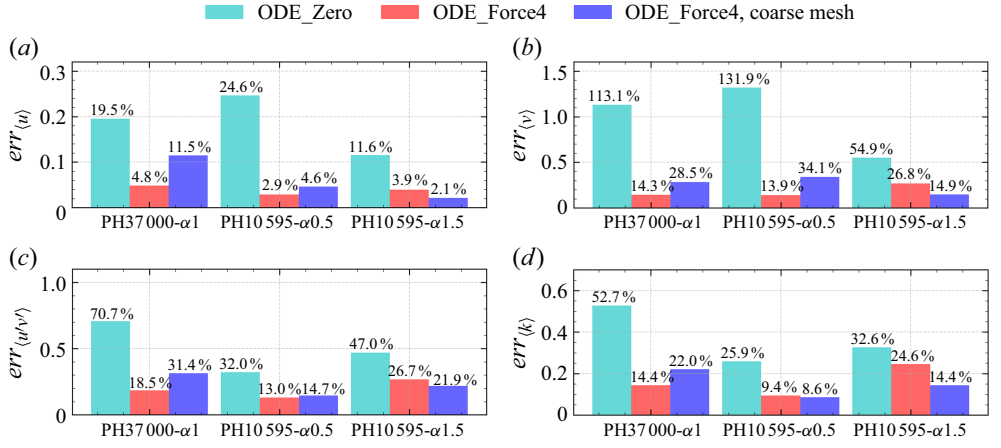


Figure 7. *A posteriori* tests using the periodic hill cases. Relative errors computed using (4.1) for (*a*) time-averaged streamwise velocity, (*b*) time-averaged vertical velocity, (*c*) primary Reynolds shear stress and (*d*) turbulence kinetic energy.

effects due to pressure gradient and flow separations are encapsulated in an overarching nonlinear force. The forcing term, which is composed of basis functions with their coefficients modelled using neural networks, is additively learned in a case-after-case manner. The data from each case defines a set of flow states. When adding new training flow data, the applicable flow state space for the model is enlarged. To ensure the model's accuracy at various flow states, a distance function is introduced to the coefficients of the forcing term.

The proposed approach was tested using turbulent channel flows across a range of Reynolds numbers, flows over periodic hills with varying Reynolds numbers and hill

https://doi.org/10.1017/jfm.2025.361 Published online by Cambridge University Press

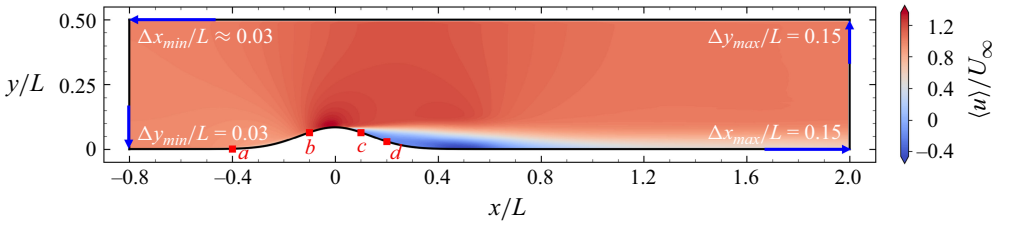


Figure 8. Contour of time-averaged streamwise velocity for wall-modelled LES of the 2-D Gaussian bump case. The ODE_Force4 wall model is employed. Red square markers (a,b,c,d) denote the positions at $x/L = -0.4$, -0.1, 0.1 and 0.2, respectively, for comparison with experimental results.

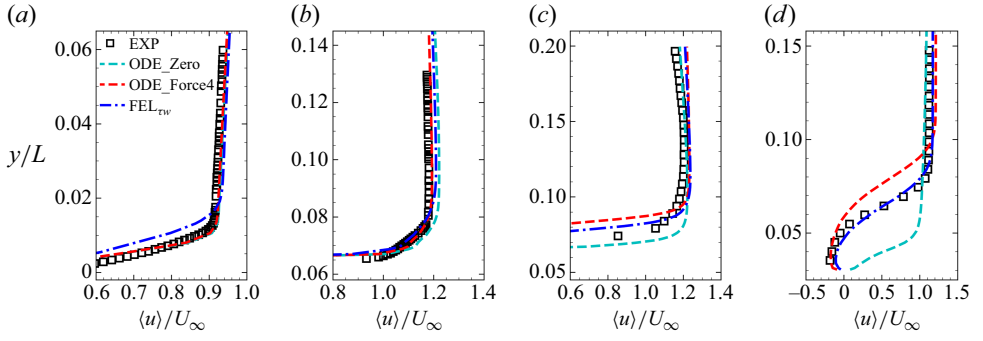


Figure 9. Test of the learned model using the 2-D Gaussian bump case for vertical profiles of the time-averaged streamwise velocity at various streamwise locations, i.e. (a) $x/L = -0.4$, (b) $x/L = -0.1$, (c) $x/L = 0.1$ and (d) $x/L = 0.2$. The reference experimental data (EXP) are from Gray *et al.* (2022). The FEL$_{\tau_w}$ data are from Zhou *et al.* (2025).

slopes, and the flow over a 2-D Gaussian bump. The *a priori* tests showed that the proposed approach can additively learn a wall model with increasing capabilities in predicting the wall shear stresses for varying flow states. The *a posteriori* tests demonstrate the capability of the learned wall model in accurately predicting both attached flows and separated flows with varying surface curvatures and Reynolds numbers.

Acknowledgements. The authors thank the anonymous reviewers for their valuable comments, which greatly improved the quality and clarity of this paper.

Funding. This work was supported by the NSFC Basic Science Center Program for 'Multiscale Problems in Nonlinear Mechanics' (no. 11988102), the Strategic Priority Research Program of Chinese Academy of Sciences (CAS, no. XDB0620102), the National Natural Science Foundation of China (nos 12172360, 12002345) and CAS Project for Young Scientists in Basic Research (YSBR-087).

Declaration of interests. The authors report no conflict of interest.

References

Arranz, G., Ling, Y., Costa, S., Goc, K. & Lozano-Durán, A. 2024 Building-block-flow computational model for large-eddy simulation of external aerodynamic applications. *Commun. Engng* **3** (1), 127.

Bin, Y., Chen, L., Huang, G. & Yang, X.I.A. 2022 Progressive, extrapolative machine learning for near-wall turbulence modeling. *Phys. Rev. Fluids* **7** (8), 084610.

Bobke, A., Vinuesa, R., Örlü, R. & Schlatter, P. 2017 History effects and near equilibrium in adverse-pressure-gradient turbulent boundary layers. *J. Fluid Mech.* **820**, 667–692.

https://doi.org/10.1017/jfm.2025.361 Published online by Cambridge University Press

BOSE, S.T. & PARK, G.I. 2018 Wall-modeled large-eddy simulation for complex turbulent flows. *Annu. Rev. Fluid Mech.* **50** (1), 535–561.

CABOT, W. & MOIN, P. 2000 Approximate wall boundary conditions in the large-eddy simulation of high Reynolds number flow. *Flow Turbul. Combust.* **63** (1/4), 269–291.

CHOI, H. & MOIN, P. 2012 Grid-point requirements for large eddy simulation: chapman's estimates revisited. *Phys. Fluids* **24** (1), 011702.

DUPRAT, C., BALARAC, G., MÉTAIS, O., CONGEDO, P.M. & BRUGIÈRE, O. 2011 A wall-layer model for large-eddy simulations of turbulent flows with/out pressure gradient. *Phys. Fluids* **23** (1), 015101.

GRAY, P.D., GLUZMAN, I., THOMAS, F.O., CORKE, T.C., LAKEBRINK, M.T. & MEJIA, K. 2022 Benchmark characterization of separated flow over smooth Gaussian bump. In *AIAA Aviation 2022 Forum*, pp. 3342.

HE, G., JIN, G. & YANG, Y. 2017 Space-time correlations and dynamic coupling in turbulent flows. *Annu. Rev. Fluid Mech.* **49** (1), 51–70.

LEE, M. & MOSER, R.D. 2015 Direct numerical simulation of turbulent channel flow up to $Re_\tau \approx 5200$. *J. Fluid Mech.* **774**, 395–415.

LOZANO-DURÁN, A. & BAE, H.J. 2023 Machine learning building-block-flow wall model for large-eddy simulation. *J. Fluid Mech.* **963**, A35.

MANHART, M., PELLER, N. & BRUN, C. 2008 Near-wall scaling for turbulent boundary layers with adverse pressure gradient: a priori tests on DNS of channel flow with periodic hill constrictions and dns of separating boundary layer. *Theor. Comput. Fluid Dyn.* **22** (3-4), 243–260.

MILANO, M. & KOUMOUTSAKOS, P. 2002 Neural network modeling for near wall turbulent flow. *J. Comput. Phys.* **182** (1), 1–26.

PARTHASARATHY, A. & SAXTON-FOX, T. 2023 A family of adverse pressure gradient turbulent boundary layers with upstream favourable pressure gradients. *J. Fluid Mech.* **966**, A11.

PIOMELLI, U. & BALARAS, E. 2002 Wall-layer models for large-eddy simulations. *Annu. Rev. Fluid Mech.* **34** (1), 349–374.

POPE, S.B. 2000 *Turbulent Flows*. Cambridge University Press.

SLOTNICK, J.P. 2019 Integrated CFD validation experiments for prediction of turbulent separated flows for subsonic transport aircraft, In NATO *Science and Technology Organization, Meeting Proceedings RDP*, STO Publication STO–MP–AVT–307-06.

SLOTNICK, J.P., KHODADOUST, A., ALONSO, J., DARMOFAL, D., GROPP, W., LURIE, E. & MAVRIPLIS, D.J. 2014 CFD vision 2030 study: a path to revolutionary computational aerosciences. NASA Tech. Rep., NASA/CR–2014-218178.

VADROT, A., YANG, X.I.A. & ABKAR, M. 2023*a* Survey of machine-learning wall models for large-eddy simulation. *Phys. Rev. Fluids* **8** (6), 064603.

VADROT, A., YANG, X.I.A., BAE, H.J. & ABKAR, M. 2023*b* Log-law recovery through reinforcement-learning wall model for large eddy simulation. *Phys. Fluids* **35** (5), 055122.

WANG, M. & MOIN, P. 2002 Dynamic wall modeling for large-eddy simulation of complex turbulent flows. *Phys. Fluids* **14** (7), 2043–2051.

YANG, X.I.A., ZAFAR, S., WANG, J.-X. & XIAO, H. 2019 Predictive large-eddy-simulation wall modeling via physics-informed neural networks. *Phys. Rev. Fluids* **4** (3), 034602.

YANG, X.I.A., CHEN, P.E.S., ZHANG, W. & KUNZ, R. 2024 Predictive near-wall modelling for turbulent boundary layers with arbitrary pressure gradients. *J. Fluid Mech.* **993**, A1.

YANG, X.I.A. & GRIFFIN, K.P. 2021 Grid-point and time-step requirements for direct numerical simulation and large-eddy simulation. *Phys. Fluids* **33** (1), 015108.

ZHANG, F., ZHOU, Z., ZHANG, H. & YANG, X. 2022 A new single formula for the law of the wall and its application to wall-modeled large-eddy simulation. *Eur. J. Mech. - (B/Fluids)* **94**, 350–365.

ZHOU, Z., HE, G. & YANG, X. 2021 Wall model based on neural networks for les of turbulent flows over periodic hills. *Phys. Rev. Fluids* **6** (5), 054610.

ZHOU, D., WHITMORE, M.P., GRIFFIN, K.P. & BAE, H.J. 2023*a* Large-eddy simulation of flow over boeing gaussian bump using multi-agent reinforcement learning wall model. In *AIAA AVIATION. 2023 Forum*, pp. 3985. AIP Publishing.

ZHOU, Z., YANG, X.I.A., ZHANG, F. & YANG, X. 2023*b* A wall model learned from the periodic hill data and the law of the wall. *Phys. Fluids* **35** (5), 055108.

ZHOU, Z., ZHANG, X.-L., HE, G.-W. & YANG, X. 2025 A wall model for separated flows: embedded learning to improve a posteriori performance. *J. Fluid Mech.* **1002**, A3.

https://doi.org/10.1017/jfm.2025.361 Published online by Cambridge University Press